

Retinal Vessel Radius Estimation and a Vessel Center Line Segmentation Method Based on Ridge Descriptors

Changhua Wu · Jennifer J. Kang Derwent ·
Peter Stanchev

Received: 20 January 2008 / Revised: 6 March 2008 / Accepted: 14 April 2008
© 2008 Springer Science + Business Media, LLC. Manufactured in The United States

Abstract This paper studies the retinal vessel radius estimation and proposes a segmentation method for vessel center lines based on ridge descriptors. The study on radius estimation reveals that the radius estimation by the matched filters based on the second order derivatives of Gaussian kernels is only correct at the vessel center. The relation between the vessel radius and the scale of the Gaussian kernel in the estimation method based on the normalized largest curvature is also studied. The ridge descriptor proposed in this paper contains the normalized largest curvature and the orientations of gradients in the local neighborhood. For vessels of a certain scale, the distribution of the descriptors is assumed to be a normal distribution and is learned from a training set with known truth. Vessel center line segmentation can be then performed based on the distance between the ridge descriptor at candidate pixels and the learned model. Evaluation of the vessel center line segmentation based on the descriptors is done on both DRIVE and STARE databases using the receiver operating characteristic

(ROC) curves. The areas under the ROC curves on DRIVE and STARE databases are 0.9584 and 0.9421 respectively.

Keywords Retinal image · Ridge segmentation · Center line · Radius estimation · Scale space theory · Ridge descriptor

1 Introduction

Retinal fundus assessment has been widely used by the medical community for diagnosing vascular and non-vascular pathology. Inspection of the retinal vessels may reveal hypertension, diabetes, arteriosclerosis, cardiovascular disease and stroke [1]. Computer assisted image analysis of the retinal images is highly helpful in many cases. For example, the diagnosis of diabetic retinopathy, the leading cause of blindness in the West World, can be prevented with treatment at an early stage. Because of this, the World Health Organization recommends annual ocular screening, which can be greatly facilitated with the adoption of automatic tools [2].

One important task in the automated processing of retinal images is the segmentation of blood vessels. The vascular features such as radius, length, branching angle, and tortuosity have diagnostic relevance and can be used to monitor the progression of diseases [3]. For example, the vessel radius can be used to calculate the blood flow through the vessels. The change in blood flow may indicate the narrowing or growth of vessels, which is closely related to diabetes. However, accurate vessel segmentation in retinal images is difficult due to

C. Wu (✉) · P. Stanchev
Department of Computer Science,
Kettering University, Flint, MI 48504, USA
e-mail: cwu@kettering.edu

P. Stanchev
e-mail: pstanche@kettering.edu

J. J. Kang Derwent
Department of Biomedical Engineering,
Illinois Institute of Technology,
10 West 32nd Street, Chicago,
IL 60616-3793, USA
e-mail: derwent@iit.edu

several reasons: the presence of noise, the low contrast between vessels and background, variation of vessel radius, brightness, and shape. The presence of lesion, exudates, and other pathological effects may create large abnormal regions, which add to the difficulty of vessel segmentation.

Previous methods for vessel segmentation in retinal images can be generally divided into two groups [4]. The first group consists of rule-based methods, including vessel tracking [5–8], matched filter responses [9–12], grouping of edge pixels [13], model-based locally adaptive threshold [14], model-fitting [15], topology adaptive snakes [16], probabilistic filtering [17], morphology-based techniques [3, 18, 19] and Hessian eigenvalue-based multi-scale filters [20, 21]. The second group consists of supervised methods, which requires training on manually labeled images, such as the neural network scheme for pixel classification [22] and the ridge based segmentation approach by Staal [4].

The segmentation of vessels can be represented in two ways. One way is to mark out all vessel pixels. The other way is to find the vessel center lines and the radius at each pixel of the center lines. In the existing work, a couple of ways for estimating the vessel radius have been proposed. The most obvious way is to measure the distance between the parallel boundary edges of a vessel. However, the accurate localization of edges is not easy given the low contrast and noise. Methods based on the intensity profile of the cross section other than the edges have been proposed. In Chaudhuri et al. [10], the vessel radius is estimated from the standard deviation of the Gaussian kernel matched to the vessel profile. In Frangi et al. [20] and Li [21], the vessel radius is estimated from the deviation σ of the smoothing Gaussian kernel that produces the largest σ -normalized maximum second order derivative over multiple scales. In Gang et al. [11], the second order derivatives of multiple Gaussian kernels are used to convolve with the image, and the vessel radius is estimated from the deviation of the Gaussian kernel that produces the maximum adjusted convolution response. Much of the literature on vessel radius estimation only discusses the relation between the vessel radius and the deviations of Gaussian kernels at the vessel center, while the relation between them at the points away from the center line are not adequately examined.

This paper focuses on the vessel radius estimation and the segmentation of the vessel center lines. The paper examines the relation between the vessel radius and the deviations of the Gaussian kernels in two popular vessel radius estimation methods, and proposes an approach for segmenting the vessel center lines based on ridge descriptors. This paper is organized as follows.

Section 2 discusses in detail the responses of two commonly used functions in the estimation of vessel radius at pixels away from the vessel center lines and the relation between the deviation of the Gaussian kernel that produces the largest response and the vessel radius. Section 3 proposes a novel descriptor for vessel center lines. Section 5 presents an approach to segment the vessel center lines based on the distributions of ridge descriptors learned from a given training set. Section 6 discusses the experiment results and evaluates the performance of the proposed method. Section 7 concludes this paper and discusses the future work.

2 Responses of Two Commonly Used Vessel Radius Estimate Approaches

In the estimation of vessel radius, response functions based on multiple-scale convolution with the second order Gaussian functions and the normalized curvatures are widely used. In this section, the response functions of the two approaches are discussed in detail. The purpose is to have a thorough understanding of the responses not only at the vessel centers but also at pixels away from the centers.

The two response functions to be discussed are all based on the inverted green channel and the assumption that the cross-section profile of a vessel in the green channel is Gaussian after intensity inversion and that the deviation of the Gaussian profile is assumed to be equal to the vessel radius. Section 2.1 discusses the response of the convolution with the second order Gaussian derivative in the multiple-scale matched filters [11, 12] and Section 2.2 discusses the response of the normalized largest curvature commonly used in the filters based on the eigenvalues of Hessian matrix [20, 21].

2.1 Response of Convolution with the Second Order Gaussian Derivative

In the multiple scale matched filters [11, 12], retinal images are convoluted with an adjusted second-order derivative of a Gaussian function:

$$f(x) = \frac{1}{\sqrt{2\pi}\sigma^t} (x^2 - \sigma^2) e^{-\frac{x^2}{2\sigma^2}} \quad (1)$$

where t is for adjusting the power of the deviation σ . The convolution, in other words, the response at the center of a vessel with radius equal to w is [11]:

$$h(t) = \int_{-\infty}^{\infty} \frac{1}{\sqrt{2\pi}\sigma^t} (x^2 - \delta^2) e^{-\frac{x^2(w^2+\sigma^2)}{2w^2\sigma^2}} dx \quad (2)$$

The value of t affects the relation between σ and w . For some values of t , the convolution hits maximum at a particular scale and the relation between the σ of that scale and the vessel radius can be determined. More particularly, when $t = 3.5$, $h(t)$ will hit maximum when $\sigma = w$ [11]. Therefore, we can have an estimate of the radius of a vessel by convolving it with the adjusted second order derivatives of Gaussian functions at multiple scales and looking for the scale that produces the maximum response.

In the following part of this section, the relation between σ and w is further explored at pixels away from the center. Consider a point p whose distance from the vessel center is α , if we use p as the origin, the cross profile of a vessel can be described by a shifted Gaussian signal (without loss of generality, the amplitude is assumed to be 1):

$$g(x) = e^{-\frac{(x-\alpha)^2}{2w^2}} \tag{3}$$

The convolution of $g(x)$ and $f(x)$ becomes

$$F(x) = \frac{1}{\sqrt{2\pi}\sigma^t} \int_{-\infty}^{\infty} e^{-\frac{(\tau-\alpha)^2}{2w^2}} ((x-\tau)^2 - \sigma^2) e^{-\frac{(x-\tau)^2}{2\sigma^2}} d\tau \tag{4}$$

The above equation shows the responses at all positions in the cross section of a vessel. The response at p is $F(0)$:

$$F(0) = \frac{1}{\sqrt{2\pi}\sigma^t} \int_{-\infty}^{\infty} (\tau^2 - \sigma^2) e^{-\left(\frac{(\tau-\alpha)^2}{2w^2} + \frac{\tau^2}{2\sigma^2}\right)} d\tau \tag{5}$$

$$= \frac{e^{-\frac{\alpha^2(1-\sigma^2)}{2w^2}}}{\sigma^t(\sigma^2 + w^2)^{3/2}} \{-\sigma^5 w + \sigma^5 w \alpha^2\} \tag{6}$$

When considering the response at the center of a vessel, $\alpha = 0$, then

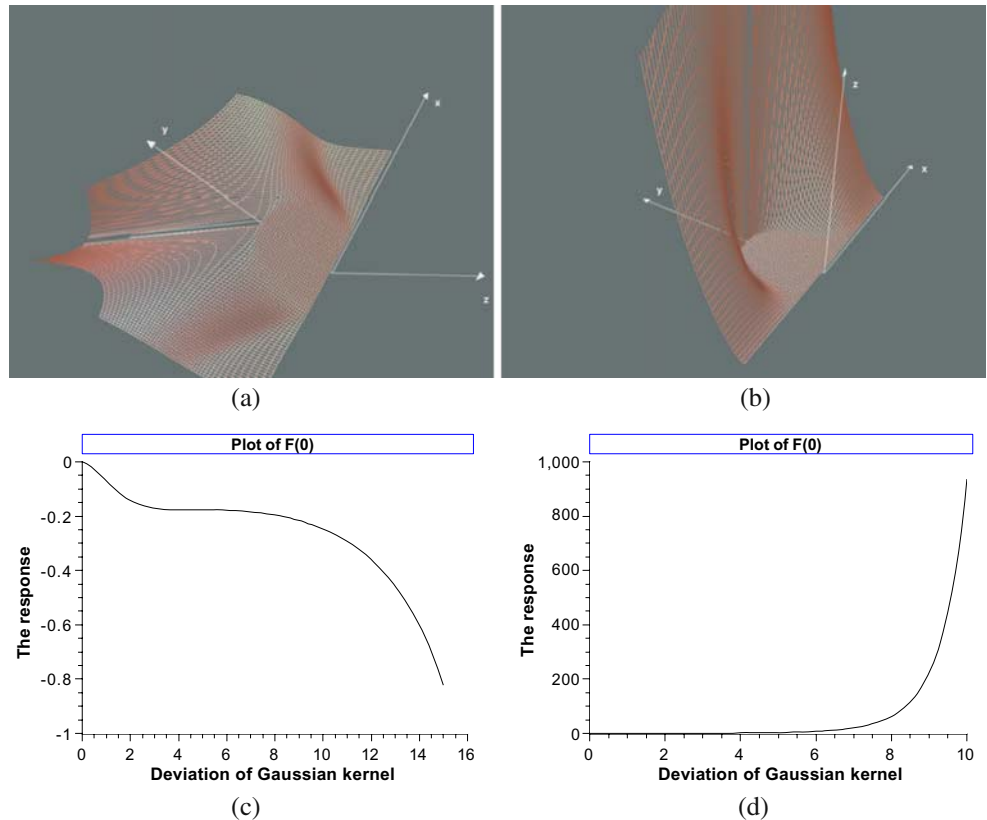
$$F(0)_{\alpha=0} = \frac{-\sigma^{5-t} w}{(\sigma^2 + w^2)^{3/2}} \tag{7}$$

$F(0)_{\alpha=0}$ will have a peak. The $\hat{\sigma}$ that produces the maximum response is dependent on t . When $t = 3.5$, w is equal to $\hat{\sigma}$ and the response at p can be expressed by

$$F(0)_{t=3.5} = e^{-\frac{\alpha^2(1-\sigma^2)}{2w^2}} \frac{\sigma^{1.5} (\alpha^2 - 1)}{(\sigma^2 + w^2)\sqrt{\left(\frac{\sigma}{w}\right)^2 + 1}} \tag{8}$$

Unfortunately, $F(0)_{t=3.5}$ does not have a maximum over σ , which means that the radius estimation of vessels is only accurate at the vessel centers. Figure 1 shows two

Figure 1 Sample rendering of $F(0)_{t=3.5}$. The first row is the 3D rendering, where x axis is the vessel radius w , the y axis is σ and z axis is the response $F(0)_{t=3.5}$. **a** α is equal to 0.5. **b** α is equal to 2. The second row is 2D drawing when particular α and w are fixed. **c** α is 0.5 and w is 3. **d** α is 2 and w is 5.



sample surfaces of $F(0)_{t=3,5}$ when α is fixed and two curves of $F(0)_{t=3,5}$ when α and w are fixed.

The fact that only the response at the vessel center has peak indicates a challenge in estimating the vessel radius using the multiple-scale matched filters. The error in detecting vessel center lines may lead to wrong or inaccurate estimates.

2.2 Response of Normalized Maximum Principal Curvature

The filters proposed in Frangi et al. [20] and Li [21] use the eigenvalues of the Hessian matrix, which is the second order derivative in the Taylor expansion:

$$I(x_0 + \delta x_0) = I(x_0) + \delta x_0^T \nabla_0 + \delta x_0^T H_0 \delta x_0 \tag{9}$$

where δx_0 is a small vector at x_0 , ∇_0 is the gradient at x_0 , and H_0 is the Hessian matrix at x_0 . H_0 is defined as

$$H_0 = \begin{bmatrix} I_{xx}(x_0) & I_{xy}(x_0) \\ I_{yx}(x_0) & I_{yy}(x_0) \end{bmatrix} \tag{10}$$

The Hessian matrix H_0 captures the second order profile at x_0 and its eigenvalues are actually the two principal curvatures at x_0 [20]. In the multiple scale filters based on Hessian matrix, the response is generally depending on the magnitude of the largest absolute eigenvalue of the Hessian matrix. For example, let $|\lambda_1| \ll |\lambda_2|$ be the two normalized eigenvalues of the Hessian matrix at scale s . The response proposed by Li [21] for two dimensional vessels is simply defined as

$$\psi_s(x) = \begin{cases} |\lambda_2| - |\lambda_1| & \text{if } \lambda_2 < 0 \\ 0 & \text{otherwise} \end{cases} \tag{11}$$

The reason for condition $\lambda_2 < 0$ is that the second order derivative of Gaussian function is negative between $-\sigma$ and $+\sigma$. The final response is the maximum of the responses on multiple scales \mathcal{T} :

$$\Psi(x) = \max\{\psi_s(x) \mid s \in \mathcal{T}\} \tag{12}$$

At each scale, the Hessian matrix is computed after smoothing the image with a Gaussian kernel. The scale \hat{s} that produces the maxima indicates the vessel radius. That is to say that there is a relation between the vessel radius and the deviation $\hat{\sigma}$ of the smoothing Gaussian kernel used at scale \hat{s} . The normalization of the eigenvalues is simply to multiply the eigenvalues by σ^2 .

The following part of this section will be dedicated to the discussion of the relation between σ and the vessel

radius w at any given point of a vessel. As we know, the convolution of two Gaussian signals produces a new Gaussian signal. Therefore, if we assume the vessel profile is Gaussian as shown in Eq. 3, then the vessel profile after the convolution is

$$f(x) = \frac{1}{\sqrt{2\pi(w^2 + \sigma^2)}} e^{-\frac{x^2}{2(w^2 + \sigma^2)}} \tag{13}$$

The curvature along the cross section of a vessel is the second order derivative of $f(x)$:

$$f''(x) = \frac{x^2 - (\sigma^2 + w^2)}{\sqrt{2\pi}\sqrt{\sigma^2 + w^2}^5} e^{-\frac{x^2}{2(\sigma^2 + w^2)}} \tag{14}$$

According to Linberg’s scale space theory [23], the eigenvalue of the Hessian matrix is normalized by σ^2 . Then the output of the filters based on the Hessian-eigenvalue is dependent on the following response R :

$$R(\sigma, x) = \sigma^2 f''(x) = \frac{\sigma^2(x^2 - (\sigma^2 + w^2))}{\sqrt{2\pi}\sqrt{\sigma^2 + w^2}^5} e^{-\frac{x^2}{2(\sigma^2 + w^2)}} \tag{15}$$

A interesting property of R is that for any value of x , R has a maximum value over σ , which means there is a particular $\hat{\sigma}$ that produces the maximum response at point x , see Fig. 2.

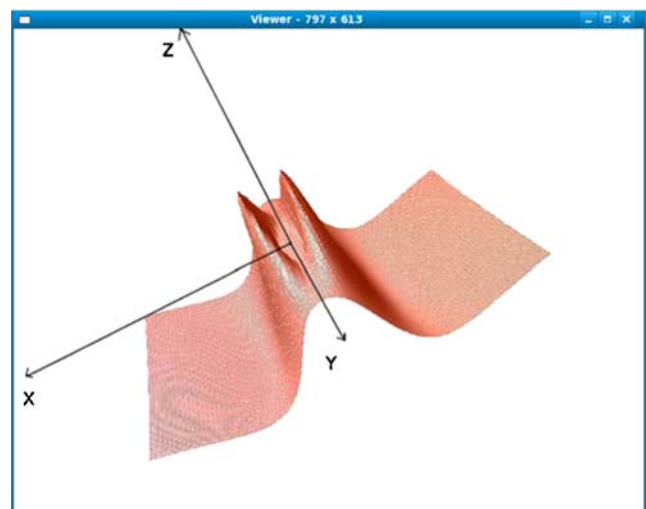


Figure 2 Sample rendering of R at a point 2 pixels away from the vessel center. x axis shows the σ , y axis shows the vessel radius, and z axis shows the value of R .

Let $\sigma^2 + w^2 = t^2$, $R(\sigma, x)$ can be rewritten as

$$R(t, x) = \frac{(t^2 - w^2)(x^2 - t^2)}{\sqrt{2\pi}t^5} e^{-\frac{x^2}{2t^2}} \tag{16}$$

$$= \frac{1}{\sqrt{2\pi}} \left\{ \left(\frac{x^2 + w^2}{t^3} - \frac{1}{t} - \frac{w^2 x^2}{t^5} \right) e^{-\frac{x^2}{2t^2}} \right\} \tag{17}$$

The t that produces the maximal $R(t, x)$ can be found at the zero-crossing of the first order derivative:

$$\frac{d(R(t, x))}{dt} = 0 \tag{18}$$

Let $A = (x^2 + w^2)t^{-3} - t^{-1} - w^2x^2t^{-5}$, we have

$$\frac{d(R(t, x))}{dt} = \frac{1}{\sqrt{2\pi}} \left(A'_t e^{-\frac{x^2}{2t^2}} + Ax^2t^{-3} e^{-\frac{x^2}{2t^2}} \right) \tag{19}$$

Therefore, Eq. 18 is equivalent to

$$A'_t + Ax^2t^{-3} = 0 \tag{20}$$

and

$$A'_t = -3(x^2 + w^2)t^{-4} + t^{-2} + 5w^2x^2t^{-6} \tag{21}$$

Plug A'_t and A into Eq. 20, and rearrange it, we get the following equation:

$$t^6 - (4x^2 + 3w^2)t^4 + (6w^2x^2 + x^4)t^2 - x^4w^2 = 0 \tag{22}$$

This is a cubic polynomial equation, whose solution is complicated and dependent on the value of w and x . However, for any particular w and x , the equation can be solved using Cardano's method (http://en.wikipedia.org/wiki/cubic_equation). The following two special cases have quite simple solutions.

- When $x = 0$, we have $t^6 - 3w^2t^4 = 0$. The solution is $t = \sqrt{3}w$. Since $t^2 = \sigma^2 + w^2$, we have $\sigma = \sqrt{2}w$, which means at the vessel center lines, the scale that uses a Gaussian kernel of deviation equal to $\sqrt{2}w$ produces the largest response.
- When $x = w$, we have $t^6 - 7w^2t^4 + 7w^4t^2 - w^6 = 0$. This equation has three roots, but only one root has practical meaning. The valid root is $t = \sqrt{3 + 2\sqrt{2}}w$. Therefore, the deviation of the Gaussian kernel that produces the largest response is $\sqrt{2 + 2\sqrt{2}}w$.

According to Cardano's method (http://en.wikipedia.org/wiki/cubic_equation), the solution for t^2 at points between the boundary and the center should be a polynomial function of x and w . For a particular vessel, w is a fixed, therefore solution for t^2 is a polynomial function

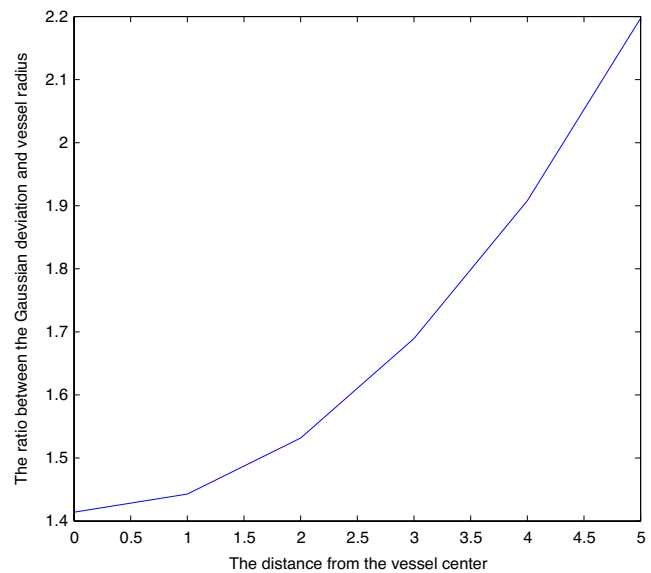


Figure 3 The ratio between the σ that produces the maximum response and the vessel radius w at points whose distances from the center are 0, 1, 2, 3, 4 and 5 pixels. The vessel radius is 5 pixels. The curve in this figure suggests that ratio is monotonically increasing.

of x only. Figure 3 shows the ratio σ/w at different values of x when w is equal to 5. It suggests that σ/w is monotonically increasing with respect to x . If so, then the σ that produces the maximum response at any point between the center and the boundary is in the range $(\sqrt{2}w \sqrt{2 + 2\sqrt{2}}w)$.

3 Ridge Descriptors

In this section, a new vessel segmentation approach based on scale-space ridge descriptors is proposed. Ridges are defined as points where an image has an extremum in the direction of the largest surface curvature. In retinal images on which experiments of this paper are conducted on, the center lines of vessels are actually overlapping with minima ridges due to the fact the vessel center has the lowest intensity in the cross section of a vessel (though some large arteriolar vessels have center reflection resulting in higher intensity in the center, center reflex can be smoothed out by large Gaussian kernels.)

From now on, minima ridges are simply referred to as ridges. The descriptor includes both the gradient orientations (Fig. 6) and the adjusted maximum eigenvalue of the Hessian matrix. The gradients are computed within an adaptive local window whose size is dependent on the vessel radius. Therefore the first step is to estimate the radius of vessels, which is obtained

using the adjusted maximum eigenvalue of Hessian matrix, defined in Eq. 15. Let σ be the deviation of the Gaussian kernel that produces the largest response, then the radius of the vessel is $\sqrt{2}\sigma$ according to the discussion in the previous section. The reason that the Hessian-based approach is chosen is that the response R has a peak value at any position away from the vessel center while the response in the multiscale matched filters does not. Since the radius of most vessels in the images in both DRIVE and STARE database is less than 6 pixels, we set the σ of the Gaussian kernels at scales from 0.5 to 6 with an interval of 0.5 to achieve subpixel accuracy. The scale selection should be dependent on the resolution of the images.

Let r be the estimated radius of a vessel, p be a pixel of a ridge, and v be the unit vector along the ridge. The local patch around p is first smoothed by a Gaussian kernel with deviation $\sigma = \sqrt{2}/2r$ for suppressing noise, then it is rotated so that the ridge is in horizontal direction. The rotation angle is simply the angle between v and the horizontal direction. After the rotation, the local patch is re-sampled at an interval of $0.20r$ in both the horizontal and vertical directions. Linear interpolation is used when the sampling point falls in between pixels. The re-sampling produces a 11×21 grid, shown in Fig. 4. The grid captures the local profile of vessels and is irrelevant to the vessel directions and scales. Therefore, it improves the accuracy of gradient computation especially for the small vessels.

The scale-space ridge descriptor is a 19 dimension vector. The first 9 elements record the orientations of gradients starting at column 3 and every other column in the second row of the grid. Similarly, the second 9 elements record the orientations of the gradients in the second row from the bottom of the grid. The last element records the maximum response of the adjusted largest eigenvalue of the Hessian matrix.

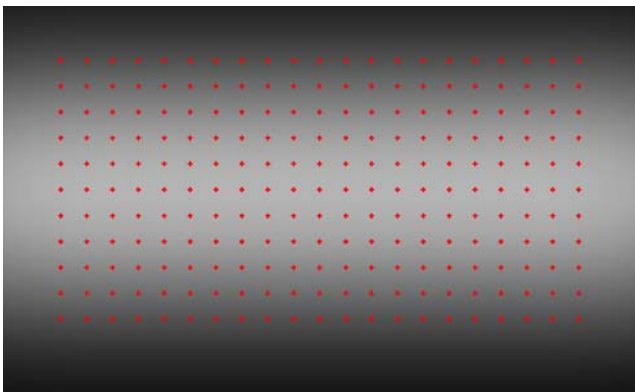


Figure 4 The grid for sampling the vessel profile.

4 The Training of Models Based on Ridge Descriptors

With the ridge descriptors, we can build a set of distribution models of the ridge descriptors and use the models for segmenting vessel center lines. Assuming that the distribution of the ridge descriptors at the center lines for vessels of each particular radius is normal. Then the mean and the covariance of the distribution can be learned from the manual vessel segmentation provided in the training set of DRIVE database.

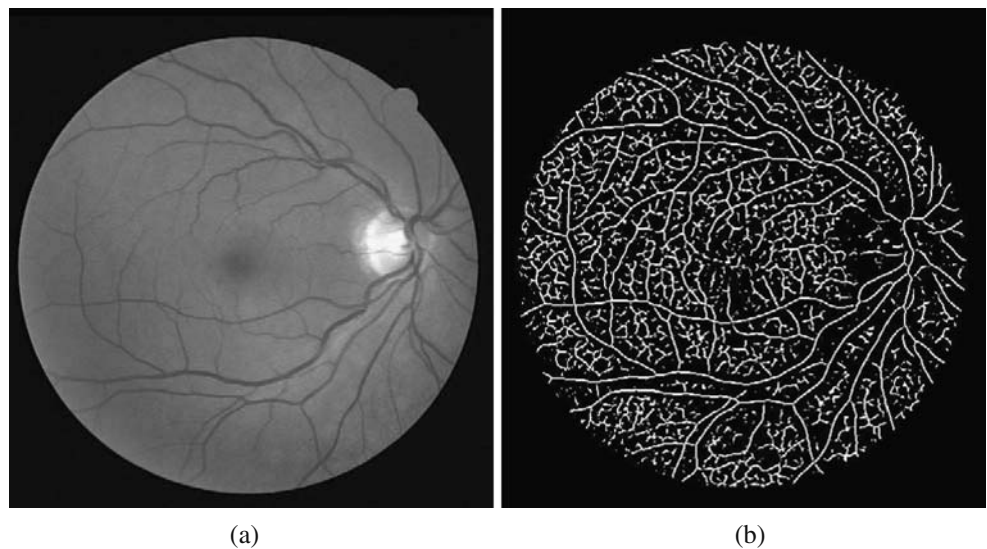
In order to build the distribution model of the ridge descriptors of the vessel center lines using the training set, the vessel center lines should be found first. The vessel center lines can be found by the checking the common pixels between the manual segmentation and the ridges. The ridge detection method used in this paper is described in Kalitzin [24]. As has been discussed earlier, ridges are defined as points where an image $I(x)$ has an extremum in the direction of the largest curvature. In other words, ridges are points in the image where the first order derivative in the direction of the largest curvature changes sign. The direction of the largest curvature is the eigenvector corresponding to the largest eigenvalue λ of the Hessian matrix H and the largest eigenvalue is the largest curvature. The sign of λ indicates whether a local minima ($\lambda > 0$) or a local maxima ($\lambda < 0$) is found. To improve the accuracy, derivatives are computed after convolving the image with a Gaussian kernel of deviation σ . Convolving the image with Gaussian kernels of various σ can be used to find the ridge of multiple scales according to the scale-space theory [23]. After computing the gradients and the eigenvalues of Hessian matrices, for each pixel x , a scalar $\rho(x, \sigma)$ can be computed as follows

$$\rho(x, \sigma) = -\frac{1}{2} \text{sign}(\lambda) |\text{sign}(\nabla I(x + \epsilon v, \sigma) \cdot v) - \text{sign}(\nabla I(x - \epsilon v, \sigma) \cdot v)| \quad (23)$$

where ∇ is a gradient operator and v is the unit-vector in the direction of the largest curvature. Parameter ϵ controls the spacial accuracy of the point set to be detected. In the continuous case, ϵ can be infinitely small. Since images are discrete, the natural choice for ϵ is 1. When $x + \epsilon v$ falls in between pixels, linear interpolation is used to get the gradient. All the image processing discussed in this paper is on the green channel of the color retinal images, since the contrast in the green channel is larger than that in the red and blue channels. Figure 5 shows the green channel of a retinal image and the ridges detected when $\sigma = 1$.

For each pixel p in the ridge, the vessel radius at p is estimated by finding the deviation of the Gaussian

Figure 5 **a** The green channel of a fundus image. The radius of the FOV is 540 pixels. **b** The local minimal ridges of **a**, $\sigma = 1.0$ pixel. Due to noise, some pixels in the center of the image are detected as ridge pixels. A subset of the ridges coincide with the vessels center lines.



kernel that produces the largest response as defined in Eq. 15. Then the ridge descriptor at p is computed. Let D_r be the set of all descriptors for ridge pixels where the vessel radius is equal to r . Then the centroid of the model for vessels whose radius is r is the mean vector of D_r and the covariance matrix of vectors in D_r is used as the covariance matrix of the model. In this way, we have built statistical models for vessels of all radius.

5 Model-Based Vessel Center Segmentation

As we can see from the training stage, the models we built is best suitable for segmenting the pixels near the center lines. We assume that with center lines segmented and radius estimated, it would be relatively easy to find all vessel pixels quite accurately. In the segmentation stage, the image is smoothed by Gaussian kernels of multiple scales and the response R is computed at each scale. If the maximum R at a pixel is positive, then this pixel becomes a candidate of ridge pixels (in retinal images, vessels are darker than background).

For each ridge pixel candidate, the ridge descriptor is computed in the same way as in the training process. Let d be the descriptor computed at pixel p and r is the estimated vessel radius at p . Then we can compare d with the corresponding model. There are two ways to evaluate the fitness between a descriptor and a given model. One way is computing the density d given the model. Due to the fact that smaller vessels are usually more subject to noise, the distribution of descriptors of small vessels are less concentrated than that of the descriptors of larger vessels. So the density would be biased in favor of the larger vessels. To eliminate this

bias, we compute the following value for each candidate given its ridge descriptor d :

$$v = (d - \mu_r) * \sum_r^{-1} * (d - \mu_r)' \tag{24}$$

where μ_r and Σ_r are the centroid and the covariance matrix of the model for vessels of radius equal to r . The magnitude of v indicates how far the descriptor at the current pixel is from the centroid μ_r . Larger v means the current pixel is more unlikely to be a pixel on a vessel center line, vice versa. Thresholding on v will provide a segmentation of the vessel center lines. For a given threshold t , all candidates whose v values are smaller than t can be marked as vessel center line pixels. According to the way the ridge descriptors are computed, if the vessel radius is r , then the vessel radius on the smoothed local patch would be $(1 + \sqrt{2}/2)r$. Since the gradients of the local descriptor are computed

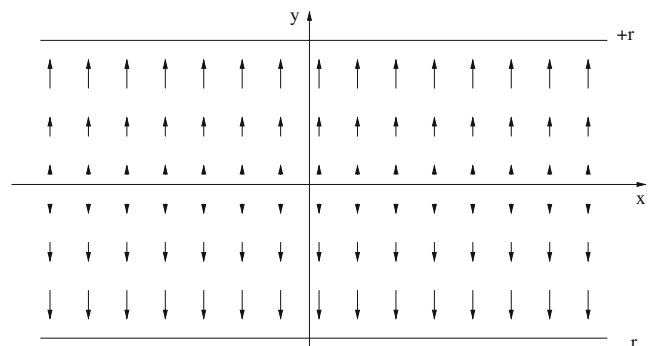
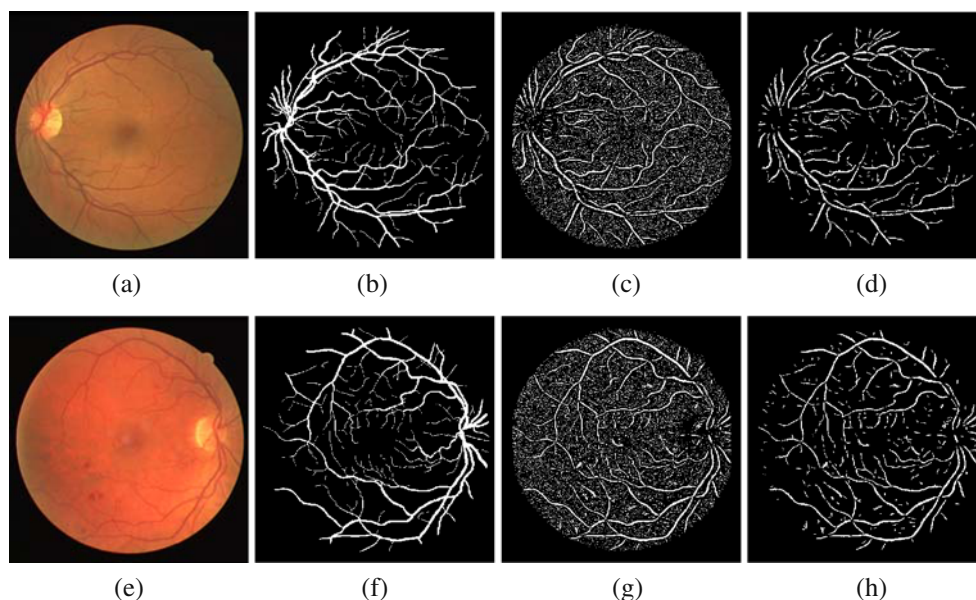


Figure 6 The gradient model of 2D vessels. The magnitude of the gradients increases from the center of the vessel to the boundary.

Figure 7 The sample segmentation results of two images in the test set of DRIVE database. The retinal images are shown in the first column (a, e). The second column is the manual segmentation (b, f). The segmentation using threshold 10 is shown in the third column (c, g). The last column shows the results after removing some small connected components (d, h).



at location of distance $0.8r$ from the sampling grid center, not only pixels on the vessel center lines but also the pixels whose distance from the center lines is no more than $(1 + \sqrt{2}/2)r - 0.8r \approx 0.58r$ are expected to have descriptors resulting low v values, therefore

being segmented as center line pixels. After removing small connected components, the final result of vessel center lines are detected by finding the common pixels in the segmentation and the detected ridge pixels using method in Section 4 (Fig. 6).

Figure 8 The segmentation results using the model trained on the training set of the DRIVE database. **a** ROC curve of the segmented vessel center lines on the DRIVE test set. The area under ROC curve is 0.9584. **b** The percentage of the center lines of small vessels segmented at each threshold level in the DRIVE database. **c** ROC curves on the STARE database. The area under the ROC curve is 0.9421. **d** The percentage of the center lines of small vessels segmented in the STARE dataset.

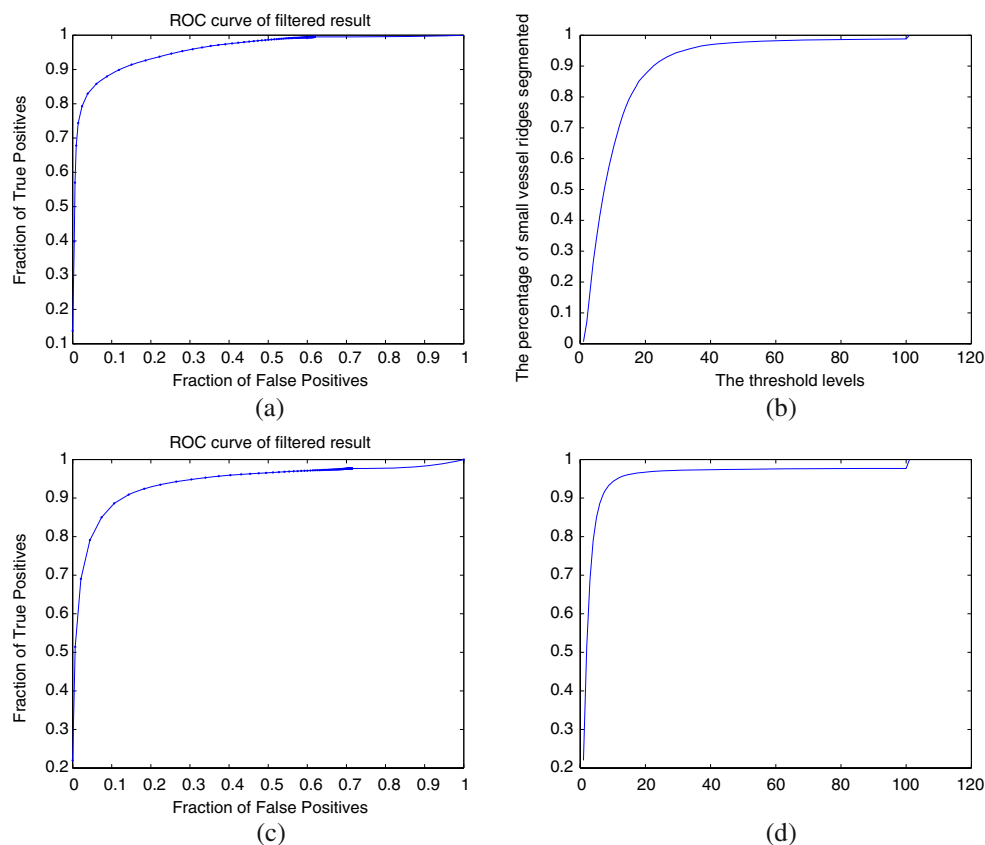


Table 1 FPs and TPs at multiple threshold levels on the test set of DRIVE database.

t	1	4	8	12	16	20	24	28
FPs	0	0.0092	0.0610	0.1865	0.3070	0.3905	0.4513	0.4927
TPs	0.1376	0.6781	0.8582	0.9266	0.9591	0.9737	0.9815	0.9857

6 Experiments

We tried the proposed segmentation method on two retinal image databases. The first database is known as DRIVE and is collected by Niemeijer [25]. DRIVE consists of 40 images (seven with pathologies) captured by a Canon CR5 3CCD camera with a 45 degree field of view (FOV). The images are of size 565*584 pixels with 8 bits per color channel. For each image, a mask image is provided that delineates the FOV. The images are divided into a training set and a test set, each containing 20 images. The test set has four images with pathologies. All images in DRIVE are manually segmented. The images in the test set were segmented twice, resulting in a set A and a set B. In set A, 12.7% of pixels were marked as vessel against 12.3% in set B. The performance of the proposed approach is evaluated on the test set using set A.

The second database is made public by Hoover [9] and is known as STARE. The STARE database consists of 20 images (10 with pathologies) captured by a TopCon TRV-50 fundus camera at 35 degree FOV. Each image has 700*605 pixels with 8 bits per color channel. All the images are manually segmented by two observers. The first observer marked 10.4% of pixels as vessel, the second one 14.9%. The performance of the proposed method is evaluated using the segmentation of the first observer as ground truth.

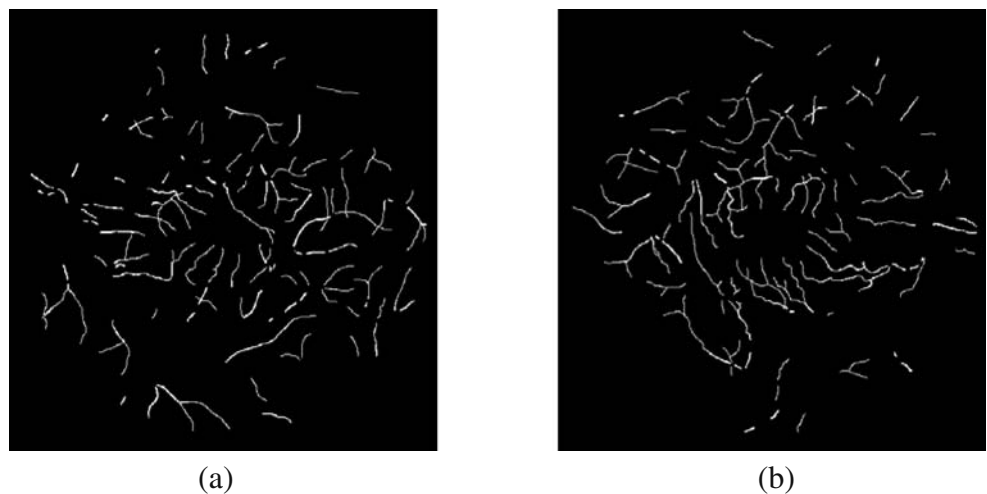
Figure 7 shows the sample segmentation results on two images in the test set of DRIVE database. The first

image is normal while the second contains pathologies. As we can see, the segmentation can find most of the vessels with small amount of false positives. In order to quantitatively evaluate the performance of the proposed approach in segmenting vessel center lines, we use receiver operating characteristic (ROC) curves. In this evaluation, the threshold t varies from 1 to 100. At each threshold level, the segmentation undergoes a small component removal process in which the small connected components are moved if they satisfy the either one of the following two conditions:

- containing less than 10 pixels
- width-to-length ratio of the bounding rectangle larger than 0.20 and containing less than 20 pixels

The connected components are found by 8-direction continuity. The ground truth of vessel center lines is obtained by finding the common pixels in the ridges detected using the method in Section 4 and the manual segmentation. The ratio between true positives and total known ridge pixels, and the ratio between false positives and total center line pixels detected by the approach are computed at each threshold level for the ROC curve. Figure 8 shows the ROC curve on images in the testing set of DRIVE database and the ROC curve on the images in STARE database using the models learned from the training set of DRIVE database. Table 1 shows the FPs and TPs at eight threshold levels t on images in the test set of DRIVE database. The

Figure 9 Small vessels of diameter less than 3 pixels obtained from the manual segmentation of two retinal images. The manual segmentation of **a** and **b** are shown in Fig. 7b and f respectively.



areas under the ROC curves on DRIVE and STARE databases are 0.95848 and 0.9421 respectively.

To evaluate the performance of the proposed approach in segmenting the center lines of small vessels, for each given manual segmentation in the test set of DRIVE database and the manual segmentation in the STARE database, a binary image that contains the vessels of diameter less than 3 pixels is created through morphological operation. Figure 9 shows two sample images of small vessels. The percentage of small vessel center lines segmented at each threshold level is shown in Fig. 8(b) and (d).

The proposed method is programmed using Matlab and experiments discussed above are carried on a HP a1710n desktop with two AMD64 processor at 2.2 Ghz and 3 GB memory. It takes 895 s to build the ridge descriptor models on the 20 images in the training set of the DRIVE database and 3360 s to compute the v defined in Eq. 24 for all ridge candidates in the 20 images of the testing set of the DRIVE database. The time cost increases quickly with the increased number of scales and the size of the smoothing Gaussian kernel at each scale.

7 Conclusion and Future Work

In this paper, the responses of two vessel radius estimation approaches at any point in the cross section of a vessel is studied. The study reveals that the response of the convolution with the adjusted second order Gaussian derivative does not have maxima except at the vessel center, and that the response of normalized maximum principal curvature has maxima at any point in the cross section of a vessel. The study indicates that for the multiple scale matched filter that uses the convolution with the second order Gaussian derivative, the radius estimate is only valid at the vessel center. For the approach that uses the normalized maximum principal curvature, the study shows the relation between the scales of the Gaussian kernels and the vessel radius is dependent on distance from the vessel center.

This paper also proposed a new vessel ridge segmentation approach based on a scale-space descriptor, which captures the normalized maximum principal curvature and the orientations of local gradients. The segmentation is based on multiple-scale models learned from a training set with ground truth given. Evaluation of the performance on images in DRIVE and STARE databases shows that the ridge-descriptor can successfully segment the vessel center lines very accurately. Most of the existing approaches focuses on the segmentation of all vessel pixels and no quantitative evaluation

on their performance in the segmentation of small vessels are given. The ROC curves on segmenting all vessel pixels can not reflect the performance on small vessels since the pixels belonging to small vessels are only a relatively small portion of all vessel pixels. While focusing on the vessel center lines, this approach proposed in this paper have demonstrated performance in segmenting the vessel center lines including the center lines of small vessels, though quantitative comparison with the existing methods are not available. The future work would be to monitor the vessel radius and the vessel growth in patients with pathologies so as to find the relation between the development of pathologies and the vessel deformation. The final goal would be early detection of certain diseases based on analyzing the retinal images.

Acknowledgements The authors would like to thank Prof. Ilya Kudish in the Department of Mathematics at Kettering University. The discussion with Prof. Kudish is very helpful.

References

1. Kanski, J. J. (1989). *Clinical ophthalmology: A systematic approach*. London: Butterworth-Heinemann.
2. Klonoff, D. C., & Schwartz, D. M. (2000). An economic analysis of interventions for diabetes. *Diabetes Care*, 23(3), 390–404.
3. Martinez-Perez, M. E., Hughes, A. D., Stanton, A. V., Thom, S. A., Chapman, N., Bharah, A. B., et al. (2002). Retinal vascular tree morphology: A semi-automatic quantification. *IEEE Transactions on Biomedical Engineering*, 49(8), 912–917, August.
4. Staal, J., Abramoff, M. D., Niemeijer, M., Viergever, M. A., & van Ginneken, B. (2004). Ridge-based vessel segmentation in color images of the retina. *IEEE Transactions on Medical Imaging*, 23(4), 501–509, April.
5. Chutatape, O., Zheng, L., & Krishnan, S. (1998). Retinal blood vessel detection and tracking by matched gaussian and kalman filters. In *Proceedings of IEEE international conference of engineering in medicine and biology society* (Vol. 20, pp. 3144–3149).
6. Tolia, Y. A., & Panas, S. M. (1998). A fuzzy vessel tracking algorithm for retinal images based on fuzzy clustering. *IEEE Transactions on Medical Imaging*, 17, 263–273, April.
7. Can, A., Turner, J., Tanenbaum, H., & Roysam, B. (1999). Rapid automated tracing and feature extraction from retinal fundus images using direct exploratory algorithms. *IEEE Transactions on Biomedical Engineering*, 3(2), 125–138.
8. Gagnon, L., Lalonde, M., Beaulieu, M., & Boucher, M.-C. (2001). Procedure to detect anatomical structures in optical fundus images. In *Proceedings of SPIE medical imaging: Image processing* (Vol. 4322, pp. 1218–1225).
9. Hoover, A., Kouznetsova, V., & Goldbaum, M. (2000). Locating blood vessels in retinal images by piecewise threshold probing of a matched filter response. *IEEE Transactions on Medical Imaging*, 19(3), 203–210.
10. Chaudhuri, S., Chatterjee, S., Katz, N., Nelson, M., & Goldbaum, M. (1989). Detection of blood vessels in retinal

- images using two-dimensional matched filters. *IEEE Transactions on Medical Imaging*, 8(3), 263–269, September.
11. Gang, L., Chutatape, O., & Krishnan, S. M. (2002). Detection and measurement of retinal vessels in fundus images using amplitude modified second-order Gaussian. *IEEE Transactions on Biomedical Engineering*, 49(2), 168–172, February.
 12. Sofka, M., & Stewar, C. V. (2005). Retinal vessel extraction using multiscale matched filters confidence and edge measures. Technical Report 05-20, The Department of Computer Science, Rensselaer Polytechnic Institute, 16 August 2005.
 13. Pinz, A., Bernogger, S., Datlinger, P., & Kruger, A. (1998). Mapping the human retina. *IEEE Transactions on Medical Imaging*, 17(4), 606–619, August.
 14. Jiang, X., & Mojon, D. (2003). Adaptive local thresholding by verification-based multi-threshold probing with application to vessel detection in retinal images. *Transactions on Pattern Analysis and Machine Intelligence*, 25(1), 131–137, January.
 15. Mahadevan, V., Narasimha-Iyer, H., Roysam, B., & Tanenbaum, H. (2004). Robust model-based vasculature detection in noisy biomedical images. *IEEE Transaction on Information Technology in Biomedicine*, 8(3), 360–376.
 16. McInerney, T., & Terzopoulos, D. (2000). T-snakes: Topology adaptive snakes. *Medical Image Analysis*, 4(2), 73–91.
 17. Wu, C., & Agam, G. (2007). Probabilistic retinal vessel segmentation. In *Proceedings of SPIE international symposium on medical imaging*. San Diego, California, February.
 18. Zana, F., & Klein, J. C. (2001). Segmentation of vessel-like patterns using mathematical morphology and curvature evaluation. *IEEE Transactions on Image Processing*, 10(7), 1010–1019 (July).
 19. Leandro, J., Cesar, J. R., & Jelinek, H. (2001). Blood vessels segmentation in retina: Preliminary assessment of the mathematical morphology and of the wavelet transform techniques. In *Proceedings of XIV Brazilian symposium on computer graphics and image processing*, (pp. 84–90), 15–18 October.
 20. Frangi, A. F., Niessen, W. J., Vincken, K. L., & Viergever, M. A. (1998). Multiscale vessel enhancement filtering. *Lecture Notes in Computer Science*, 1496, 130–137.
 21. Li, Q. (2003). Selective enhancement filters for vessels and airway walls in two- and three-dimensional CT scans. *Medical Physics*, 30(8), 2040–2051.
 22. Sinthanayothin, C., Boyce, J., Cook, H., & Williamson, T. (1999). Automated localisation of the optic disc, fovea, and retinal blood vessels from digital colour fundus images. *British Journal of Ophthalmol*, 83(8), 902–910, August.
 23. Lindeberg, T. (1998). Edge detection and ridge detection with automatic scale selection. *International Journal of Computer Vision*, 30(2), 117–156.
 24. Kalitzin, S. N., Staal, J., ter Haar Romeny, B. M., & Viergever, M. A. (2001). A computational method for segmenting topological point-sets and application to image analysis. *IEEE Transactions on Pattern Analysis and Machine Intelligence*, 23(5), 447–459, May.
 25. Niemeijer, M., Staal, J., van Ginneken, B., Loog, M., & Abramoff, M. (2004). Comparative study of retinal vessel segmentation methods on a new publicly available database. In J. M. Fitzpatrick & M. Sonka (Eds.), *Proceedings of SPIE medical imaging* (Vol. 5370, pp. 648–656). Bellingham: SPIE.



Changhua Wu obtained his Bachelor degree in Engineering and Master degree in Computer Science from Hangzhou Institute of Electronic Engineering in 1998 and 2001 respectively. Dr. Wu obtained his Ph.D degree in computer science from Illinois Institute of Technology in 2005. His current research interests include image processing, computer vision, computer graphics, human computer interface, robotics, and sensor networks. He is a professional member of IEEE and ACM.



Jennifer J. Kang Derwent is an associate professor of Biomedical Engineering at the Illinois Institute of Technology. Dr. Kang Derwent received a B.S. degree in Mathematics, a M.S. in Applied Mathematics and a Ph.D. in Biomedical Engineering from Northwestern University. Dr. Kang Derwent was a Post-doctoral Research Fellow in the Department of Ophthalmology and Visual Sciences at the University of Illinois at Chicago. Her professional research interest includes retinal electrophysiology, blood flow, ocular drug delivery and neural engineering.



Peter Stanchev is a professor at Kettering University, US, and professor and chair at the Institute of Mathematics and Informatics, Bulgarian Academy of Sciences. His research interests include multimedia systems, multimedia semantics, and medical systems. Stanchev has a PhD in mathematics and computer science from Sofia University.